



## An integrated Landsat time series protocol for change detection and generation of annual gap-free surface reflectance composites



Txmin Hermosilla <sup>a,\*</sup>, Michael A. Wulder <sup>b</sup>, Joanne C. White <sup>b</sup>, Nicholas C. Coops <sup>a</sup>, Geordie W. Hobart <sup>b</sup>

<sup>a</sup> Integrated Remote Sensing Studio, Department of Forest Resources Management, University of British Columbia, 2424 Main Mall, Vancouver, BC V6T 1Z4, Canada

<sup>b</sup> Canadian Forest Service (Pacific Forestry Centre), Natural Resources Canada, 506 West Burnside Road, Victoria, British Columbia V8Z 1M5, Canada

### ARTICLE INFO

#### Article history:

Received 27 June 2014

Received in revised form 3 November 2014

Accepted 7 November 2014

Available online 5 December 2014

#### Keywords:

Best available pixel

Change detection

Proxy value

Image compositing

Landsat

Temporal analysis

### ABSTRACT

Mapping and monitoring land cover and land cover change remains a top priority for land managers. Uniquely, remote sensing offers the capacity to acquire information in a systematic (spatially, temporally, and categorically) and synoptic fashion that is appealing from monitoring and reporting perspectives. The opening of the Landsat archive and new processing and analysis opportunities enable the characterization of large areas and the generation of dynamic, transparent, systematic, repeatable, and spatially exhaustive information products. Best Available Pixel (BAP) approaches enable the production of periodic image composites free of haze, clouds, or shadows over large areas. In this paper we demonstrate an integrated protocol to produce spatially exhaustive annual BAP image composites that are seasonally constrained and free of atmospheric perturbations. These annual BAP composites for the years inclusive of 1998 to 2010 provide for generation of a suite of change metrics for the period 2000 to 2010 using Landsat Thematic Mapper (TM) and Enhanced Thematic Mapper Plus (ETM+) data. The study area is the >375,000 km<sup>2</sup> forested area of Saskatchewan, Canada. We evaluate the robustness of the protocol by comparing in-filled (or proxy) values with a true reference set for surface reflectance. An initial change detection pass is used to aid in the allocation of proxy values (for missing and anomalous values) and to allocate change events to the correct year, with a second pass to characterize key change points and related time series trends (e.g., change year, post-change slopes, among others). In so doing, a multi-temporal data cube (via a series of annual proxy composites) and a set of change metrics are generated. Approximately 35% of the pixels in our study area required proxy values, either as a result of missing data or our noise detection approach. Overall, our results indicate strong agreement between the assigned proxy values and the reference data ( $R = 0.71\text{--}0.91$ , RMSE = 0.008–0.025). Agreement was stronger for pixel series with no change events ( $R = 0.73\text{--}0.92$ , RMSE = 0.007–0.024), relative to pixel series with change events ( $R = 0.63\text{--}0.87$ , RMSE = 0.010–0.029). The generated change metrics, derived via temporal and spatial analysis of the annual BAP composites, were an important precursor to the generation of valid proxy values, and – importantly – provide valuable information for the further assessment and understanding of land cover and land cover change. Our results indicate that the demonstrated protocol provides a reliable approach to generate proxy image composites containing no data gaps, along with a suite of informative change metrics that provide a comprehensive characterization of land cover changes (including disturbance and recovery) allowing for an improved understanding of landscape dynamics. The protocol is efficient and may be applied over large areas to support regional and national mapping and monitoring activities.

Crown Copyright © 2014 Published by Elsevier Inc. All rights reserved.

### 1. Introduction

Up-to-date land cover and change information is required by resource managers and decision-makers at regional, national, or global level to support the development and implementation of policies, and to meet mandatory reporting requirements resulting from those policies (Townshend et al., 2011). Within forest environments, information to support forest inventories has historically relied on the interpretation

of aerial images and forest plot data, providing a mix of cost effectiveness and information content typically required to support forest management activities at the strategic level. The collection and interpretation of aerial images in support of forest inventories has traditionally been implemented on a cycle, often decadal or longer to inform managers at the regional and jurisdictional level as well as to support systematic reporting on a defined suite of attributes over time, including the occurrence and extent of both anthropogenic and non-anthropogenic change. At the operational level, forest managers are increasingly using Light Detection And Ranging (LiDAR) to derive forest structure information, often with targeted digital photography

\* Corresponding author.

E-mail address: [txomin.hermosilla@live.forestry.ubc.ca](mailto:txomin.hermosilla@live.forestry.ubc.ca) (T. Hermosilla).

to meet immediate management and planning needs (Wulder, Bater, Coops, Hilker, & White, 2008). These intensive and information rich approaches are especially suitable for meeting detailed operational needs (e.g., road placement, individual tree harvesting, exclusion of sensitive environments, etc.); however, over large areas and to meet strategic inventory and jurisdictional reporting needs, other remote sensing approaches may be preferred.

For larger forested nations, such as Canada, composed of both managed and unmanaged forest lands and having multiple jurisdictions involved in stewardship, the opportunity to collect information in a systematic (spatially, temporally, and categorically) and synoptic fashion is desirable from monitoring and reporting perspectives. The opening of the Landsat archive and the associated processing and analysis opportunities (Hansen & Loveland, 2012) enables the characterization of the entire area of interest systematically with the same information source, thereby allowing for the transparent, systematic, and repeatable production of spatially exhaustive information products. Additionally, utilization of Landsat data allows for capitalization upon the rich applications and processing base that has developed over the life of the satellite program (Cohen & Goward, 2004; Wulder et al., 2008). Landsat has the longest continuous global-coverage image archive, acquired at temporal and spatial resolutions suitable for monitoring and mapping human activity and impacts (Wulder, Bater, Coops, Hilker, & White, 2008; Wulder, White, et al., 2008).

The production of national level image composites provides unique opportunities for large area characterizations, yet challenges exist. Using Canada as an example, with an area of almost 10 million km<sup>2</sup>, there are more than 1200 scenes (i.e., Worldwide Reference System-2 [WRS-2] path/rows), multiplied by the temporal depth of the Landsat archive (White & Wulder, 2013). As a result, large numbers of images must be obtained, processed (e.g., to deal with cloud and shadow), and stored. Additionally, due to the requirements to derive products (e.g., land cover, land-cover change, forest structure) with phenological fidelity, a date range for acceptable imagery is defined (e.g., mid-summer, centered on peak photosynthetic activity). This level of specificity can result in data gaps, such as when there are no cloud-free pixels found during the defined date range. The more restrictive the date requirements imposed to build the Best Available Pixel (BAP) composites, the more radiometrically consistent the vegetation phenological response is over multiple years. Increasing the temporal restrictions, however, will decrease the likelihood of obtaining suitable cloud-free images (White et al., 2014). Furthermore, the cloud masking and haze scoring routines applied are not perfect, which can result in spectral inconsistencies making it through to a given composite.

A number of novel pixel-based compositing methodologies have been proposed to derive large area image composites from multiple Landsat scenes (Flood, 2013; Griffiths, Linden, Van Der Kuemmerle, & Hostert, 2013; Hansen et al., 2011; Potapov, Turubanova, & Hansen, 2011; Roy et al., 2010). These pixel-based selection approaches implement a set of rules to guide the compositing process, and facilitate the development of techniques for regional to global land cover and land cover change monitoring applications (Hansen & Loveland, 2012) while also mitigating the creation of boundary artifacts due to mosaicking independently processed scenes (Kennedy, Yang, & Cohen, 2010). The production of annual composites thus enables creation of wall-to-wall, multi-year image time series (White et al., 2014).

Once seasonal or annual BAP composites have been developed, a time series of pixel values (hereafter referred to as a pixel series) can be derived for each pixel location through the entire time period considered. These pixel series can be used to identify, describe, and quantify changes in land cover and land-cover disturbances (Cohen et al., 2002; Griffiths et al., 2013; Huang et al., 2010; Jönsson & Eklundh, 2004; Kennedy, Cohen, & Schroeder, 2007). Ideally a pixel series would be completely populated and composed of values that meet all the requirements for inclusion in the composite, e.g., nearness to target DOY, no cloud, cloud shadow, or haze, and no missing data due to the Scan

Line Corrector failure (SLC-off). In reality, however, a pixel series may be missing values in particular years, resulting in data gaps in the pixel series that might limit the applicability of many existing data analysis methods, which generally assume fairly complete data (Lou & Obradovic, 2011). A pixel series may be characterized as stable (e.g., mature forest) or could be irregular due to changes or transitions in cover types over time. Variations in pixel values through time can also occur as a result of undesired residual clouds and shadows, undetected haze, or changes in solar illumination (Kennedy et al., 2010; Vicente-Serrano, Perez-Cabello, & Lasanta, 2008), resulting in noise or anomalous values that may impact subsequent image analyses. Both data gaps and anomalous values in the pixel series need to be addressed before the pixel series can be used for applications such as characterizing land cover and land cover change.

Our objective is to present and demonstrate a protocol to generate annual large-area BAP composites that contain no spatial or temporal data gaps (hereafter referred to as proxy value composites) and that are sufficiently spectrally consistent to enable the subsequent characterization of land cover, land cover change, and vertical forest structure. Using annual BAP image composites (described in detail in White et al., 2014) as a starting point, our approach to generating proxy value composites is novel in that we first detect spectral change, derive a series of metrics characterizing these spectral changes, and then use these change metrics to aid in proxy value assignment. As part of our protocol, we also identify any noisy or anomalous pixel values and then replace these values with proxy values. We apply the protocol to a 15 year span of imagery (1998 to 2012) to inform on a decade of 2000–2010 of forest change occurring over the forested area of Saskatchewan, Canada. We describe each component of the protocol and assess the quality of the proxy composites using a true reference set for reflective bands. The change metrics produced are presented and discussed. We conclude with recommendations focused on the application of the protocol for regional land cover mapping applications.

## 2. Background

### 2.1. Pixel-based image compositing

Pixel-based image compositing approaches constitute a new paradigm in image processing, emerging as result of the opening of the Landsat archive combined with the increasing data storage and processing capabilities (White et al., 2014). As a consequence, users now can gather long temporal series of images covering large-areas, instead of being restricted to single scenes (Loveland & Dwyer, 2012). Common to the pixel-based image compositing approaches is the selection of BAP from a set of images subject to multiple criteria. Higher scores are assigned to those pixels with more desirable conditions. Those pixels with the highest scores are included in subsequent composite development. The result is that users can apply the rules that are most appropriate to their particular information needs and produce BAP composites containing atmospheric-corrected reflectance values covering large areas.

The main difference between pixel-based image compositing approaches is their treatment of pixels that are missing suitable observations in a specific target year. Three types are distinguished: single-year, multi-year, and proxy composites (White et al., 2014). Single-year composites only use images from the target year and pixels with no suitable observations are labeled as "no data" (Roy et al., 2010), resulting in composites without complete coverage. Multi-year composites use data from alternative years (generally previous or next) when no suitable observations are found in the target year (Griffiths et al., 2013). However, off-year imagery might negatively impact the study of vegetated areas (Brooks, Thomas, Wynne, & Coulston, 2012) by hindering the analysis of trends and detection of changes. Proxy composites are developed to overcome these limitations. This approach fills in data gaps by considering the full spectral information

of the pixel-series and replacing these pixels with synthetic values that are the most spectrally similar in time and space.

## 2.2. Noise Removal Techniques

Noise detection methods using a temporal series of data often avail upon the situation that noise-related fluctuations in spectral response are punctual and ephemeral, with an expectation that the spectral response will return to a value close to the pre-fluctuation scenario in the post-fluctuation year (Kennedy et al., 2010). In the case of image compositing, noise can be related to undetected cloud or cloud shadow, as well as haze or smoke (Fig. 1). Given a stable trajectory of pixel values through time for an undisturbed pixel of a given land-cover type, a range of expectation may be determined. Anomalous values or noise result in a surface reflectance value for the pixel in a given year which exceeds this expectation, but which clearly does not represent a change event. Replacement of these anomalous values is desired to enable production of seamless, spatially exhaustive, annual proxy value composites that are sufficiently spectrally consistent to support the production of land cover and forest structure information products.

A number of approaches have been used to detect noise in time series of remotely sensed data comparing the deviation between actual observations and model predicted values, including iterative least squares fitting (Zhu, Woodcock, & Olofsson, 2012; Zhu & Woodcock, 2014), Fourier analysis (Geerken, Zaitchik, & Evans, 2005; Roerink, Menenti, & Verhoef, 2001), harmonic analysis (Meisner, Bittner, & Dech, 1999); and pseudo-invariant feature regression (Vicente-Serrano et al., 2008). Some techniques are based upon the identification of outliers as observations with coefficients of variation exceeding a threshold and having the greatest absolute difference compared to the average value in an indicated time period (Ju, Roy, Shuai, & Schaaf, 2010). All of these approaches present some challenges that may limit their use (Jönsson & Eklundh, 2004) including the need for *a priori* determination of threshold values and analysis periods. In addition, fitting methods may be problematic when applied to irregular or asymmetric data, provoking spurious oscillations in time series (Chen, 2004). Pixels that are identified as having anomalous values or noise are assigned a “no data” value and are then filled with a proxy value. The proxy values are not measured directly, but rather are informed by other Landsat measures, such as those from preceding and/or following dates.

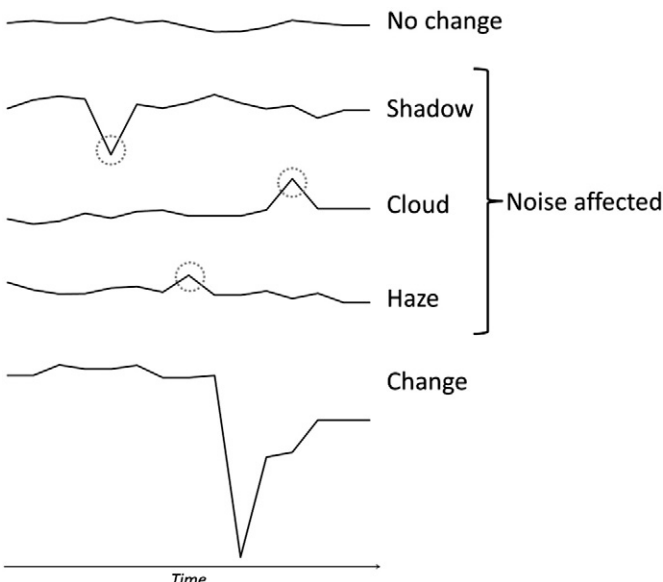


**Fig. 1.** Spectral values for pixel series with no change events, pixel series with noise related to shadow, cloud, or haze, and pixel series with change events.

## 2.3. Infill techniques for data gaps (proxy values assignment)

The application of a rule-base for producing annual image composites may result in pixels with persistent “no data” values. These data gaps represent pixels for which there is no imagery that meets the specified compositing criteria; however, based on knowledge of the pixel's value through time, these pixels can be assigned a proxy value. Due to an expectation that spectral data for a given pixel are autocorrelated over time, the information of preceding and succeeding dates has been a common approach infill data gaps. Techniques are often based on fitting oscillating functions to characterize the seasonality of the observations, e.g. least squares (Jönsson & Eklundh, 2004) or Fourier analysis (Brooks et al., 2012; Roerink et al., 2001). These approaches typically require multiple observations per year and may perform poorly when using a single observation per year. Linear interpolation techniques can also be applied to infill missing data (Keogh, Chu, Hart, & Pazzani, 2001); however, this method may result in smoothing or removal of significant trends within the time series, with likely impacts on the quality of the final composites. The most successful approaches designed to overcome these challenges examine the overall temporal pattern within the pixel series and fitting partial trends which describe the low frequency behavior of inter-annual time series (Tomé & Miranda, 2004) and allow the identification of steps or breakpoints in the series that represent disturbances and land-cover condition changes (Huang et al., 2010; Kennedy et al., 2010; Verbesselt, Hyndman, Zeileis, Culvenor, & Newnham, 2010). These breakpoints provide the key time intervals of change that delimit piecewise-based interpolations of the different trends composing a time series.

## 3. Study area and data

Development and testing of our protocol for generating seamless multi-temporal pixel-based image composites was undertaken over the forested region of the Canadian province of Saskatchewan, which has an area of 378,818 km<sup>2</sup>, representing 58% of the total area of the province (Fig. 2). This forested region is divided into three ecozones: Boreal Plains, Boreal Shield, and Taiga Shield (Rowe, 1996). More northern areas are composed primarily of black spruce (*Picea Mariana*) and jack pine (*Pinus banksiana*) and are dominated by large wildfires. These areas are considered unmanaged, meaning that there is no fire suppression or tenure arrangements for harvesting in these areas, and that there is little in the way of forest inventory information available. In contrast, more southerly latitudes of the forested area are dominated by aspen (*Populus tremuloides*), white spruce (*Picea glauca*), and tamarack (*Larix laricina*) and are subject to forest management practices (including fire suppression) with ongoing tenure arrangements allowing for harvest, with forest inventory information available for some of this area. Additionally, although fire suppression is more common in the managed forest, wildfires are still an annual occurrence.

The temporal window for protocol development was 2000 to 2010; however two additional years were added at the beginning and end of the time series to enable proxy value assignment and avoid missing data in the outermost dates of the period of interest, and to allow trends to be based upon pre- and post-period evidence as the case may be. All available images with less than 70% cloud cover from the United States Geological Survey archive of Level-1-Terrain-Corrected (L1T) Landsat Thematic Mapper (TM) and Landsat Enhanced Thematic Mapper Plus (ETM+) covering the study area that were acquired from August 1st ± 30 days from 1998 to 2012 were considered candidates for creating the image composites. The forested area of Saskatchewan is represented by 50 scenes (path/rows) of the Landsat Worldwide Referencing System. August 1st is DOY 213 and was selected as a central date with a to general correspondence with the growing season for the majority of Canada's forested ecosystems (McKenney, Pedlar, Papadopol, & Hutchinson, 2006). As the focus of this monitoring work and current methods

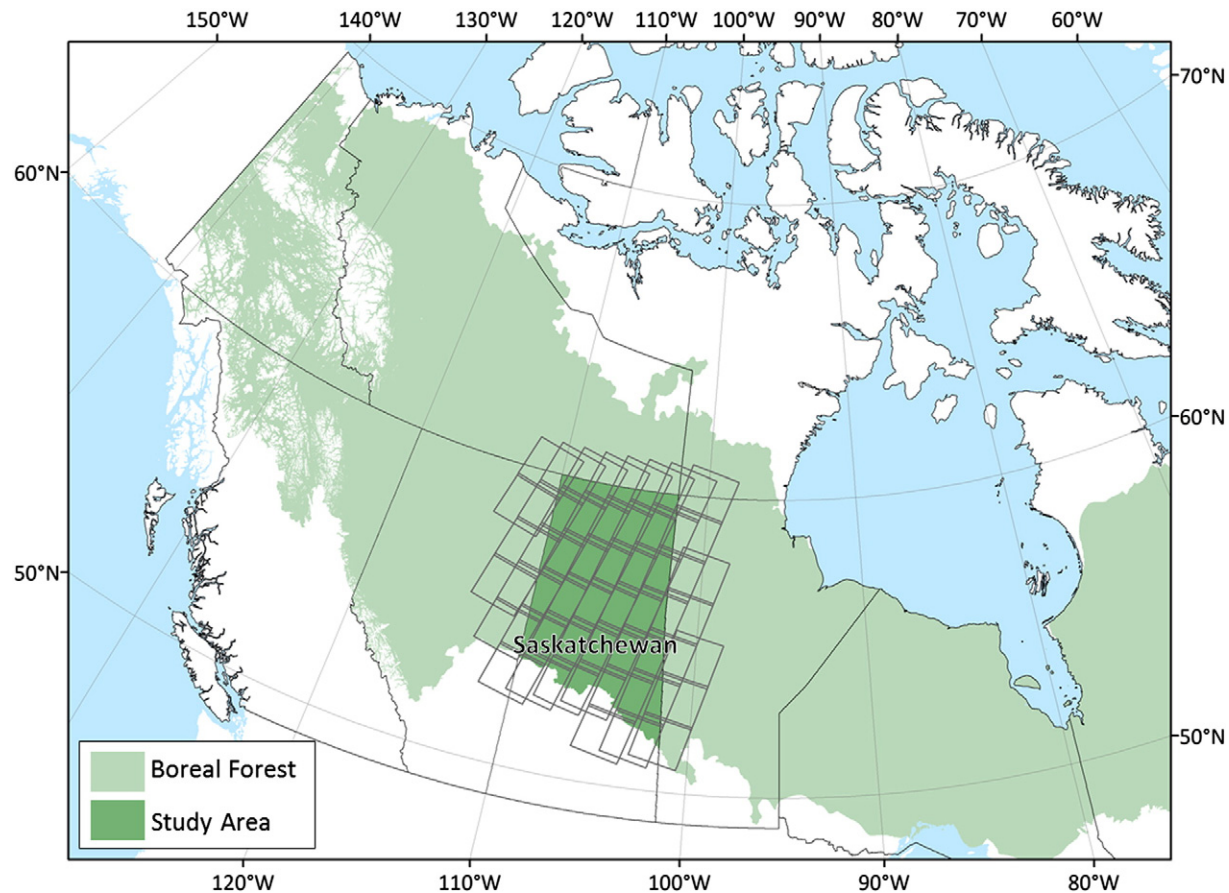


**Fig. 2.** Location of the study area (>375,000 km<sup>2</sup>) within the Canadian boreal forest. Footprints of the 50 Landsat WRS-2 scenes used are shown.

development is on forested ecosystems, agricultural lands were identified and excluded from our analyses using a mask provided by Agriculture and Agri-Foods Canada (2011 data; [ftp://ftp.agr.gc.ca/pub/outgoing/aesb-eos-gg/Crop\\_Inventory/](ftp://ftp.agr.gc.ca/pub/outgoing/aesb-eos-gg/Crop_Inventory/)).

#### 4. Methodology

We use annual BAP image composites as the initial inputs to our protocol (see workflow in Fig. 3). The methods used to generate these

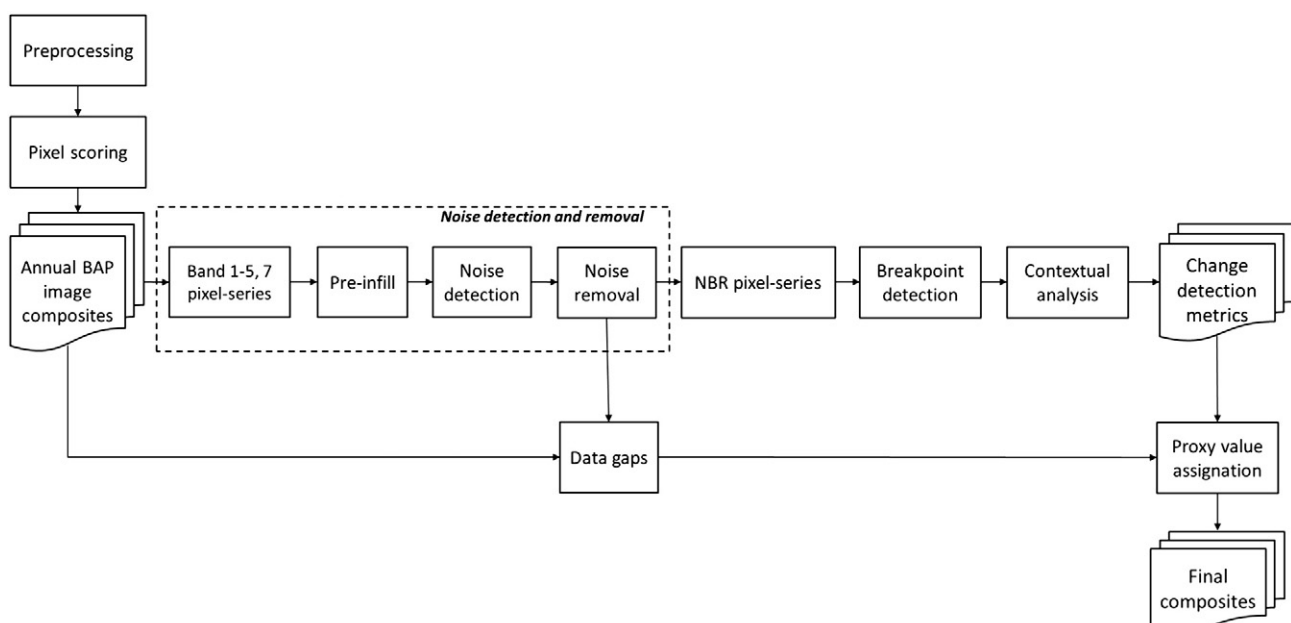


**Fig. 3.** Workflow of the proposed protocol for image compositing of dense temporal series.

annual BAP composites (including equations for scoring pixel observations) are described in detail in White et al., 2014 and therefore we provide only a brief description of them here. The protocol applied herein begins by identifying pixel locations in the annual BAP composites with observations from images acquired outside  $\pm$  30 days of the target DOY and assigning them to a “no data” value. Likewise, noisy or anomalous pixel values (i.e., pixel values that exceed a range of expectation as defined by the values in the pixel series; Fig. 1) are identified and assigned a “no data” value. This process is repeated for each year, resulting in a temporal stack of annual BAP image composites ready for subsequent processing. We then applied breakpoint analysis to each pixel series to identify spectral changes in the trajectory of surface reflectance values through time. These spectral changes are often indicative of change events such as forest disturbance or recovery, and knowledge of these events is a necessary precursor to assigning an appropriate proxy value to pixels with “no data”. In order to characterize change events, breakpoints in the pixel series are detected and analyzed in both the temporal and spatial domains. These breakpoints are used to establish the temporal interpolation limits in the time series within which to determine the applicable trend for proxy value assignment. Each of these processing steps is explained in more detail below.

#### 4.1. Generation of annual BAP image composites

As described in detail in White et al. (2014), annual BAP image composites are generated using a series of pre-processing functions. Atmospheric correction was applied to all images using the Landsat Ecosystem Disturbance Adaptive Processing System (LEDAPS) algorithm (Masek et al., 2006; Schmidt, Jenkinson, Masek, Vermote, & Gao, 2013) to transform digital numbers into surface reflectance values for the six Landsat optical bands. Clouds and their shadows were detected and masked using the Function of mask (Fmask) algorithm (Zhu & Woodcock, 2012). The Fmask was also used to generate a water mask, excluding these features from additional processing (Lunetta, Johnson, Lyon, & Crotwell, 2004). Once pre-processing is complete, scores are calculated and assigned for each pixel observation. Each pixel received four separate scores – based on modifications to those proposed by (Griffiths et al., 2013) for (i) sensor, (ii) acquisition day of year, (iii) distance to clouds and cloud shadows, and (iv) atmospheric opacity. The scores are summed and the best observation for each pixel is selected as the one with the highest score. Some of the scores operate at the image level, meaning all pixels in an image receive the same score (i.e., sensor and acquisition day of year), while other scores are pixel specific (i.e., distance to clouds and cloud shadows, and atmospheric opacity). The surface reflectance value for the “best” observation is then written out to the annual BAP composite. Details on the pixel scoring rules and annual BAP development can be found in White et al. (2014).

#### 4.2. Noise detection and removal

The first step in our protocol takes the annual BAP image composites and detects and removes noisy observations or anomalous values from the image composite. Temporal trajectories of values for a given pixel are used to define a range of expectation. Some variation in these values is expected through time, but anomalies may occur as a result of clouds or cloud shadows that are missed by the automated cloud masking routine, or by haze or other factors. It is necessary to identify these anomalous values and distinguish them from more marked spectral differences in the pixel series that may be indicative of a change event. Each pixel series is assessed to detect outliers using the filtering method proposed by (Kennedy et al., 2010), where values for a given time are examined in relation to their previous and subsequent spectral values. This outlier analysis is applied to all six Landsat spectral bands. A pixel is flagged as noise and set to “no data” when it meets two conditions: first, it is detected as an outlier; second, the difference between the

spectral value under consideration and the average of previous and subsequent values in the pixel-series exceeds a threshold – derived by sensitivity analysis – in three or more of the six bands.

#### 4.3. Assessment of data gaps

We assessed the prevalence of temporal gaps (pixels with “no data”) in the annual BAP image composites, and tracked whether these gaps resulted from the scoring functions used to generate the composite (i.e., no suitable imagery was available for a given pixel location) or whether the gap was the result of our noise detection process (i.e., the pixel's value exceeded a range of expectation determined by its pixel series and was flagged as noise). Gaps were also mapped to identify locations in our study area with persistent absence of data.

#### 4.4. Preliminary infill of data gaps

As indicated above, it is likely that some pixels will have no observations. Furthermore, pixels identified as having noisy observations will likewise have been assigned “no data” value. In order to enable the detection of spectral change events, and to avoid interpolation across potential breakpoints that are indicative of such events, a preliminary infill of pixel values is undertaken. These preliminary proxy values are derived by individually examining each year within a pixel series. The spectral value of the preceding or following year is assigned to the examined year based on the lowest standard deviation of the two years preceding or the two years following the examined year, as Eq. (1) indicates.

$$x_t = \begin{cases} \mu_{\{x_{t+1}; x_{t+2}\}} & \text{if } \sigma_{\{x_{t+1}; x_{t+2}\}} \leq \sigma_{\{x_{t-1}; x_{t-2}\}} \\ \mu_{\{x_{t-1}; x_{t-2}\}} & \text{if } \sigma_{\{x_{t+1}; x_{t+2}\}} > \sigma_{\{x_{t-1}; x_{t-2}\}} \end{cases} \quad (1)$$

where  $x_t$  is the year in the pixel series to be preliminary infilled, and  $\{x_{t-1}; x_{t-2}\}$  and  $\{x_{t+1}; x_{t+2}\}$  are the two preceding and the two following years containing data, respectively.

#### 4.5. Breakpoint detection and generation of change metrics

A breakpoint represents a change in the temporal development of a pixel's values through time. Robust identification of breakpoints enables the assignment of final proxy values to pixels with missing observations, as well as enabling change events, and the year in which the event occurred, to be correctly identified. The breakpoint detection process is performed over the Normalized Burn Ratio (NBR) (Key & Benson, 2006) pixel series, which has been demonstrated as sensitive and consistent for the retrieval of disturbance events over forest environments (Kennedy et al., 2010).

Breakpoints were detected using a variation of the bottom-up algorithm proposed by (Keogh et al., 2001). This process is composed of four main steps:

- i. Initially  $n - 1$  segments are created in a pixel series composed of  $n$  values.
- ii. Cost in terms of root-mean-square error (RMSE) of merging each pair of adjacent segments is computed.
- iii. The pair of segments with the lowest cost is merged.
- iv. The cost is recomputed for the new segments, and the process is iterated until certain stopping criteria are fulfilled.

Two stopping criteria are used, which are required prior to calculation: the maximum number of segments and the maximum merging cost allowed. During the iteration process the maximum merging cost value can be dynamically adapted to enforce the algorithm to meet the maximum number of segments requirement. The maximum number of segments was set to 5, and the maximum merging cost 0.125. An absolute maximum merging cost was chosen to avoid challenges

of defining costs relative to the time series values as discussed by Kennedy et al. (2010).

The trends computed after implementation of the breakpoint detection process are of four distinct types (Fig. 4): monotonic trends (i.e., trends with no breakpoints) (Fig. 4a); trends composed of multiple breakpoints all with positive slope segments (Fig. 4b); trends with a single breakpoint and a negative slope (Fig. 4c); and trends composed of multiple breakpoints, with at least one negative slope (Fig. 4d). From these trends, segments, and breakpoints, we derived a set of descriptive change metrics that allowed us to characterize the change events as well as conditions pre- and post-change (Table 1). Metrics relay information on change year, magnitude, persistence, and rate and are grouped into pre-change (Fig. 4d,  $\bar{s}_1$ ), change (Fig. 4d,  $\bar{s}_2$ ), and post-change (Fig. 4d,  $\bar{s}_3$ ) categories. Change metrics characterize the negative segments ( $\bar{s}_3$ ) using: date (year), persistence, magnitude, and change rate. Of particular utility to proxy value assignment, are change year (e.g., represented by breakpoint B in Fig. 4d), and change persistence (e.g., number of years between breakpoints B and C in Fig. 4d).

#### 4.6. Contextual analysis of the change events

The next step of the protocol analyzes spectral change events in the spatial domain to improve the consistency and spatial homogeneity of detection. Since changes are detected in the temporal domain (i.e., from the temporal trajectory of the pixel series), the pre-infill process of data gaps described earlier may result in spatially discordant disturbance events labeled with an incorrect year for change. If we consider discrete events, such as a wildfire, the information need is to ensure that these change events are allocated to the correct year and

have spatial cohesion with neighboring pixels of the same event. To mitigate these errors, a contextual analysis of the disturbances is undertaken in the spatial domain. It is assumed that if a change event is detected in a year with no or few data gaps, and the previous and subsequent years also have no or few data gaps, then the change event has been labeled with the correct year. We rank the reliability change detection based on data absence where the chances of correctly predicting the year of a change event is inversely related to the number of years of missing data in the pixel's trajectory. Thus, change detection reliability is ranked according to data availability in the years before, during, and after the change event.

Detected change events are spatially aggregated into pixel segments based on their date of occurrence and duration (i.e., persistence). Segments missing less than 50% of observations in a given year – before, during and after the change event – are deemed reliable and attributed with their date of occurrence. Segments that are missing more than 50% of observations in any of the considered years are ranked less reliable. Lower-ranked segments that are spatially-adjacent (eighth-connected neighborhood) to a higher-ranked segment within  $\pm$  one year are attributed the year of occurrence of the more reliable neighbor. In addition, during this process, change events that have a size less than the minimum mapping unit (MMU) are removed. The MMU size was determined to support the information needs of Canada National Forest Inventory (0.5 ha).

#### 4.7. Final infill of data gaps and generation of proxy image composites

The final step of the protocol involves assignment of final proxy values to pixels with no observations. These proxy values are computed

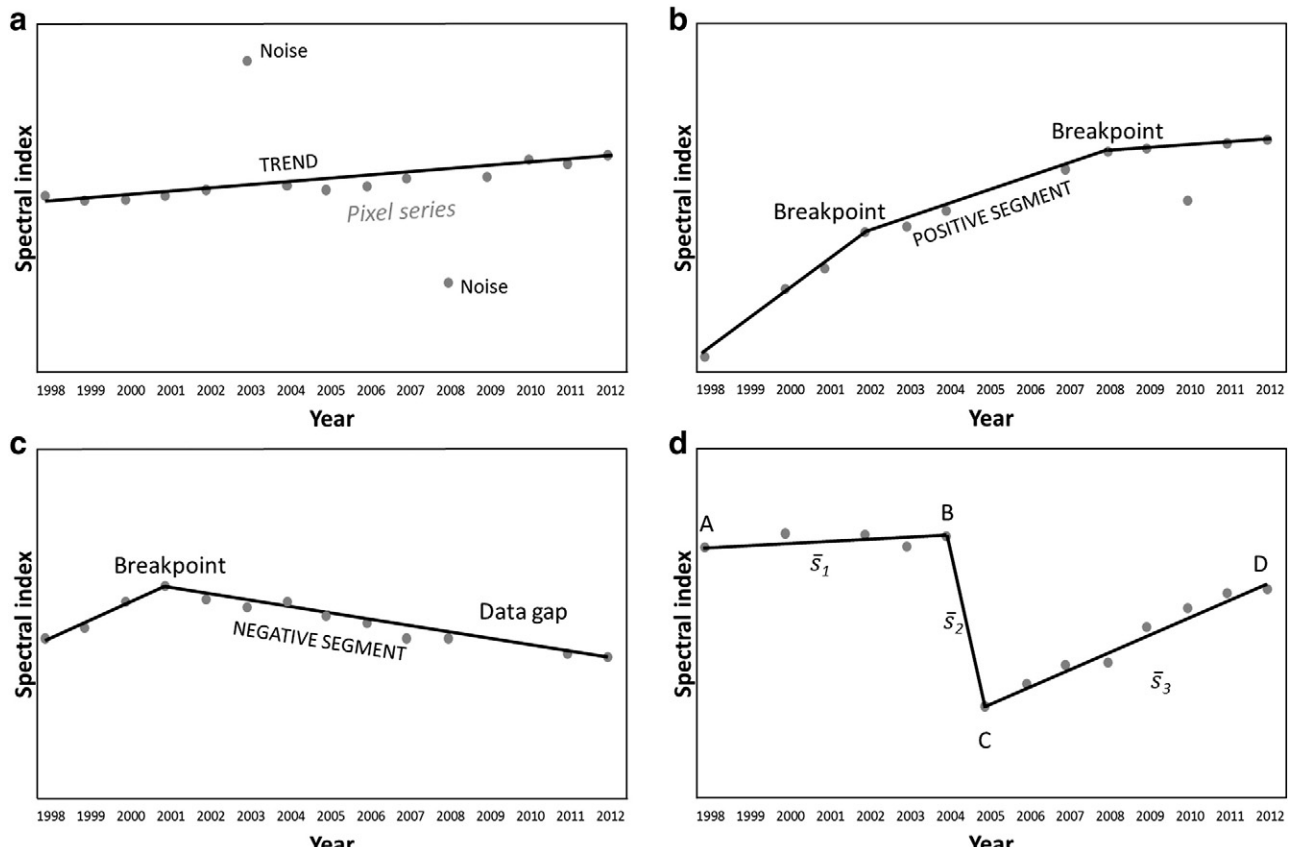


**Fig. 4.** Graphical depiction of trends computed from the pixel-series and their components: (a) monotonic, (b) multiple breakpoints all with positive slopes, (c) single-breakpoint; and (d) multiple-breakpoint (showing breakpoints – A, B, C, D – and segments –  $\bar{s}_1$ ,  $\bar{s}_2$ ,  $\bar{s}_3$  –). Adapted from Pflugmacher et al., 2013).

**Table 1**

Change metrics generated (see also Fig. 4d).

Metric	Description
Pre-change	Pre-change magnitude variation Pre-change persistence Pre-change evolution rate
Change (negative segments)	Change year Change persistence Change magnitude variation Change rate
Post-change	Post-change magnitude variation Post-change persistence Post-change evolution rate

using a piecewise linear interpolation from the temporal segments, in which breakpoints and trends have been identified and characterized, as follows:

$$x_t = x_{t-1} + (x_{t+1} - x_{t-1}) \cdot \frac{t-(t-1)}{(t+1)-(t-1)} \quad (2)$$

where  $x_t$  is the proxy value assigned to a pixels with no observation at the year  $t$ , and  $x_{t-1}$  and  $x_{t+1}$  are the spectral values in years with observations before ( $t-1$ ) and after ( $t+1$ ), respectively. Proxy values to pixels located in the extremes of the temporal segments are computed using linear extrapolation, as indicated in Eq. (3):

$$x_k = x_{k-1} + (x_k - x_{k-1}) \cdot \frac{t-(k-1)}{(k)-(k-1)} \quad (3)$$

where  $x_k$  and  $x_{k-1}$  are the spectral values of the two nearest years,  $k$  and  $k-1$ , with observations. As result, the proxy value assigned to a data gap is uniquely a function of the spectral values of the temporal segment where the gap is located. Thereby, combining information from the different trend components can be avoided, preserving so the change events in the temporal series.

#### 4.8. Assessment of proxy values

To assess the impact of our proxy value assignment process, we randomly selected 0.005% (116,000) pixels (from all cover types) that had valid pixel observations from each annual composite. We masked and flagged these pixels as “no data”, thereby generating synthetic gaps, and applied our full protocol as described above. We then assessed the final proxy surface reflectance values against the original surface reflectance values (hereafter referred to as the reference values). Proxy and references values were compared using a correlation coefficient ( $R$ ), root mean square error (RMSE), bias, and coefficient of variation (CV). For each band and group, the correlation coefficient indicates the degree of association between the reference and proxy values, the RMSE indicates the average difference between the reference and proxy values, and the bias indicates if the proxy values are typically higher or lower than the reference values. The CV is useful for comparing among different groups, but not among different spectral bands, as it provides an indication of the differences between the proxy and reference values relative to the mean reference value for a band. Bias, RMSE and CV were calculated as follows:

$$Bias_b = \frac{1}{n} \sum_{i=1}^n (Reference_{b,i} - Proxy_{b,i}) \quad (4)$$

$$RMSE_b = \sqrt{\frac{1}{n} \sum_{i=1}^n (Reference_{b,i} - Proxy_{b,i})^2} \quad (5)$$

$$CV_b = \frac{RMSE}{\bar{X}_{Reference_b}} \times 100 \quad (6)$$

where  $Reference_{b,i}$  and  $Proxy_{b,i}$  are, respectively, the reference and proxy values for each pixel in band  $b$ ,  $n$  is the number of samples, and  $\bar{X}_{Reference_b}$  is the mean spectral value for band  $b$ . Statistics were computed for all spectral bands, and were also stratified by various conditions. First we considered three distinct groupings: all pixels, pixels without change events, and pixels with change events. Secondly, we considered the impacts of an increasing number of data gaps, as well as consecutive numbers of data gaps, on the quality of the proxy value assignment.

## 5. Results

### 5.1. Assessment of data gaps

The proportion of pixels with missing data in the annual image BAP composites across the study area (not including pixels identified as water bodies) ranged from a minimum of 0.5% in 2001 to a maximum of more than 31% in 2010 over the analysis period (see Fig. 5a). On average, 15% of each annual image composite had data gaps resulting from our scoring functions (i.e., acquisition DOY, distance to cloud and cloud shadow, opacity, and sensor score). By comparison, an average of 7.5% of pixels in each annual image composite were flagged as noise, with 2001 being the year with the lowest proportion of noisy pixels (5.8%) and 2002 the year with the greatest proportion of noisy pixels (9.6%). When combined, data gaps resulting from our scoring functions and noise removal process impacted more than 35% of pixels in the years 2004, 2006, and 2010. Approximately 3.5% of the pixels in the study area did not have any gaps in any of the annual composites (Fig. 5b) and more than 50% of the pixels had three or fewer years of missing data. 99.95% of pixels had at least three years of data in the entire 11-year time series. As indicated in Fig. 5c, data gaps were often spatially concentrated, occurring more commonly in the northern portion of the study area, and this area was more prone to cloud cover, haze, and smoke from wildfires.

### 5.2. Breakpoint detection and generation of change metrics

The characterization of trends in pixel series values, the detection of breakpoints, and the generation of descriptive change metrics are an important precursor to assigning appropriate proxy values to fill in data gaps. Within our study area, the total changed area per year, grouped by the persistence of the change event, is summarized in Fig. 6. The average annual total area of change (2000–2010) is 3936 km<sup>2</sup>, with a standard deviation of ± 2920 km<sup>2</sup>. The area of change oscillates markedly and exceeds 6000 km<sup>2</sup> in 2002, 2006, 2008, and 2010. Most of the change events are of short duration, and persist only for a single year. Fig. 7 shows the persistence of the change events for 1 to 4 years or longer (Fig. 7a), and the spatial distribution of change events by year (2000–2010) across the study area (Fig. 7b).

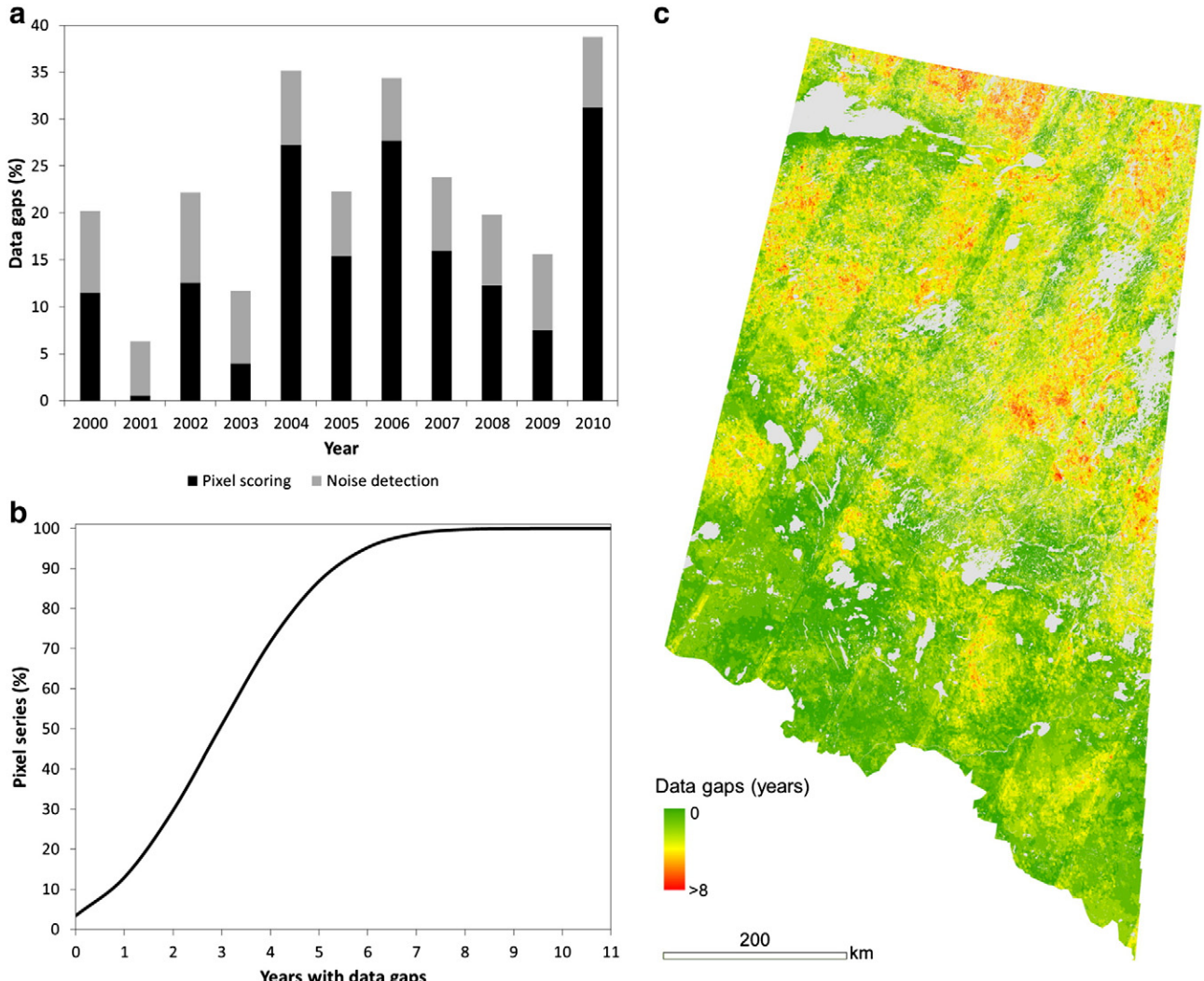


**Fig. 5.** (a) Percentage and origin of data gaps in the study area for the target years 2000–2010, and (b) cumulative histogram and (c) spatial distribution of both pixel-scoring and noise-detection data gaps along the study area (water bodies are masked).

The northern part of the study area is dominated by large change events that persist for a single year (e.g., wildfires) whereas, in the southern part of the study area, disturbances are smaller and in some locations persist for multiple years (e.g., forest harvesting).

Fig. 7c shows the magnitude of the disturbance events (i.e., the difference between spectral values at breakpoints C and B in Fig. 4d).

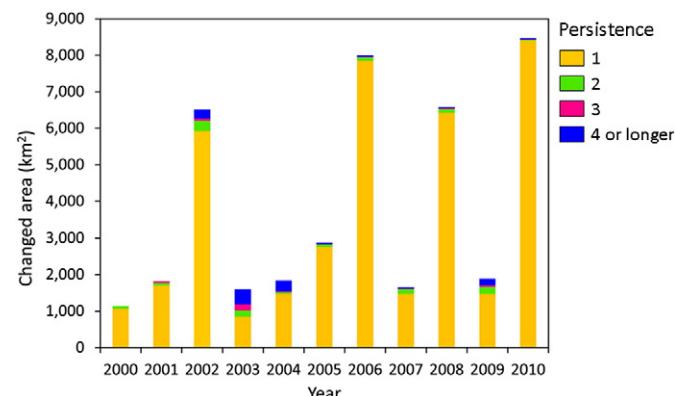


**Fig. 6.** Total changed area by year and persistence.

Change magnitude metrics provide insights regarding change severity. The values of the magnitude metric vary from 0 to –2 (corresponding to the maximum possible difference between two NBR values) and lower values are related to higher severity change processes since they are indicative of greater changes in vegetation condition and/or amount of vegetative cover. In our study area, higher severity change events are located in the central part. Fig. 7d displays the rate of recovery after the major change event expressed in NBR magnitude increase per year (i.e. the difference between spectral values at breakpoints D and C divided by the time between these breakpoints in Fig. 4d). Values close to zero represent very slow recovery processes, whereas higher values are related to increased post-disturbance regrowth.

### 5.3. Generation of proxy image composites

The protocol presented was used to generate annual proxy image composites for each year from 2000 to 2010 as shown in Fig. 8. Fig. 9 shows a sample of outputs generated from each major phase of the protocol for years 2004 to 2007: the annual BAP composite resulting from the scoring functions (with data gaps); the data gaps generated during the noise detection and removal phase; and finally, the infilling of data gaps using proxy values. As shown in 2004, and to a lesser extent 2005, the noise detection and removal process is useful for mitigating

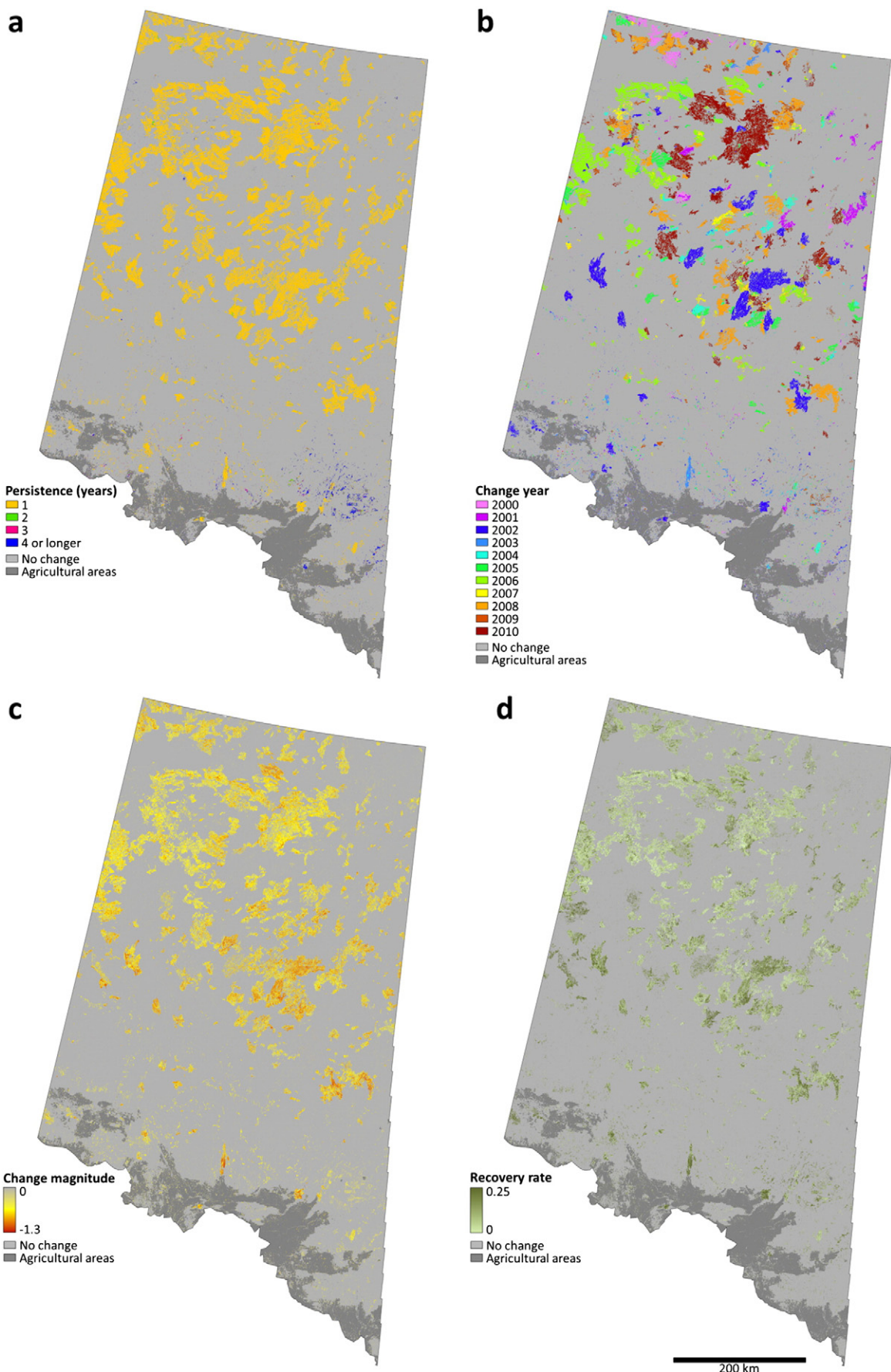


**Fig. 7.** Change events labeled by: (a) persistence, and (b) year of occurrence. (c) Change magnitude distribution. Although values of this metric vary from 0 to  $-2$  (corresponding to the maximum possible difference between two NBR values), color ramp has been adjusted from 0 to  $-1.3$  for display purposes. (d) Vegetation recovery rate after a major change event.

the effects of remaining clouds, haze, or for 2004, smoke from wildfires, the latter of which may be more challenging to detect using Fmask. Likewise, the performance of the proxy value infilling process is evident in 2006 where most of the area was missing data as a function of the BAP scoring and the noise removal process. The proxy values for 2006 reproduce a consistent spectral response of the vegetation cover resulting from the application of the piecewise linear interpolation, which prevented the mixing of spectral information from years preceding and succeeding the actual change event (i.e., a salt-and-pepper effect whereby some pixels have values pre-change, some have values post-change). Fig. 10 shows the contextual analysis component of the protocol. In the example shown, a wildfire occurred in 2002, however, as a result of the scoring functions and noise removal processes, most of the 2002 image is missing data, and the disturbance is not completely visible until 2003. Consequently, using the breakpoint detection approach without the spatial component would lead to assignment of the incorrect date (i.e. 2003, not 2002), allowing for the correct reconstruction of the spectral response of the disturbance event in the proxy values assigned to fill data gaps.

#### 5.4. Assessment of proxy values

Reference and proxy values are plotted in Fig. 11. The correlation coefficient, RMSE, bias, and CV resulting from a comparison of reference and proxy values are summarized in Table 2. Comparisons were made for three groups: all pixels combined, pixel series with no change events, and pixel series with change events. Overall, the measures indicate a strong level of agreement between surface reflectance reference values and proxy values ( $R = 0.71\text{--}0.91$ ,  $\text{RMSE} = 0.008\text{--}0.025$ ). Correlations between proxy and reference values were generally lower for pixel series with change events (0.63–0.87) compared to correlations for pixel series with no change events (0.73–0.92). Across all groups considered,  $R$  and  $\text{RMSE}$  were typically lower for bands 1, 2, and 3 (average  $R = 0.75$ ; average  $\text{RMSE} = 0.009$ ), when compared to bands 4, 5, and 7 (average  $R = 0.87$ ; average  $\text{RMSE} = 0.022$ ). Bias was slightly positive for all bands with the exception of band 4, for which the bias was consistently negative. Bias was relatively consistent across the three groups considered, with the exception of bands 5 and 7, which had a higher positive bias for pixels with change events. On average, the CV was higher for pixel series with change events (average  $\text{CV} = 23.23$ ), compared to pixel series with no change events (average  $\text{CV} = 17.09$ ).

Reference and proxy values were also assessed in the context of the number of data gaps and number of consecutive data gaps (Table 3). Here we report results for band 4 only, but other spectral bands exhibited similar trends. As the number of data gaps in a pixel series increases, the correlation between proxy and reference values decreases. A similar trend in declining correlation is seen in pixel series with consecutive data gaps, but the rate of decline is greater and includes a negative correlation at 10 years of consecutive data gaps. Trends in bias and CV are likewise greater and more volatile for pixel series with consecutive data gaps. Bias is relatively small and negative until 8 or more years of consecutive data gaps occur, at which point the bias became larger and positive.

## 6. Discussion

In this paper we describe a protocol to produce annual proxy value BAP image composites, generated using Landsat TM and ETM + data, which have no spatial or temporal gaps, and that are largely void of anomalous reflectance values and can inform on change over time. We applied the protocol to a decade of Landsat data in the boreal forest region of Saskatchewan, Canada. To restrict the spectral range related to vegetation phenology and seasonality, we defined a consistent date range corresponding with the growing season for the majority of

Canada's forested ecosystems. The date range could be modified for other applications (White et al., 2014). For example, the date range could be refined and dynamically adapted based on latitude (Zhou et al., 2001) or by identifying peak vegetation greenness using high temporal-resolution sensors such as MODIS.

When we assessed data gaps in our stack of annual BAP image composites, we found that for a single year, up to 35% of pixels of the study area required proxy value assignment, either because the pixels had data gaps resulting from a lack of suitable imagery to satisfy the BAP compositing rules, or because of noise (i.e., pixels that exceeded a range of expectation based on other values in the pixel's trajectory). Due to the long life of Landsat 5, the effective temporal revisit for Landsat has been 8 days from the beginning of Landsat 7 ETM + collections in 1999 to the demobilization of Landsat 5 TM in January 2013. While the two sensors have offered many opportunities for collecting data at a given location, the potential for data gaps has become more prevalent as of 2003 due to the SLC-off status of the Landsat 7 ETM + sensor, with the strong geometric fidelity of the ETM + instrument resulting in a high degree of spatial alignment of the SLC-off portions of imagery over time (Hansen et al., 2011).

The assignment of appropriate proxy values is enabled by first detecting and characterizing spectral change within each pixel series. This phase of the work is centered on the protocol description, with a later phase to fully assess the change detection and metrics described herein. We defined temporal segments – based on the detection of spectral changes in the temporal domain – using piecewise linear interpolation. In addition, we considered the spatial domain by applying contextual analysis to these spectral changes. The application of the contextual analysis procedure reduces possible errors in the date assigned to a given change event (i.e., breakpoint) by relabeling the change event detected in the time series based on the presence of data gaps. To do this, reliability of detected change events is ranked based on the presence of data gaps in the pixel series. The date (year) of a change event for any given pixel is reallocated to the date of a neighboring pixel's change event if the neighboring pixel is more reliable within a given time interval. The contextual analysis thereby results in the change event polygons with improved spatial contiguity and consistency. Therefore, by using both the temporal (via piecewise linear interpolation) and the spatial (via contextual analysis) domains to improve the assignment of proxy values, we are able to preserve the spectral response and temporal fidelity of the change events (as shown in Fig. 10).

The results of the proxy value assessment indicate that overall, there is a strong level of agreement between reference surface reflectance values and proxy values. However, the level of agreement varied by spectral band, and by the presence of change events and data gaps in the pixel series (Tables 2 and 3). Lower correlations and lower RMSE values were found for bands 1, 2, and 3 compared to bands 4, 5, and 7. Bias was small and positive for all bands except band 4, which had a negative bias. Differences between these bands most likely result from atmospheric effects, which are known to impact the shorter spectral wavelengths more markedly than the Landsat bands in the infrared and mid-infrared (Liang, Fang, & Morisette, 2002). Not surprisingly, it is more difficult to generate an accurate proxy value when change events and data gaps are present in the pixel series. On average, pixel series with change events had a lower correlation between proxy and reference values (0.76 versus 0.85 for no change pixels), a higher RMSE (0.019 versus 0.012), a greater bias (0.0005 versus 0.0002), and a larger CV (23.23 versus 17.09) (Table 2). Data gaps – years for which there are no data available that meet the BAP criteria – likewise have a negative impact on the generation of proxy values (Table 3). Correlation, RMSE, and CV are relatively stable until there are 5 or more years with data gaps and trends are similar for consecutive years of data gaps. Bias however has a different trend: after 8 or more years with consecutive data gaps, bias changes from being small and negative, to large and positive. Many years of consecutive data gaps may be of greatest concern in areas that are very dynamic (i.e., that have a large amount

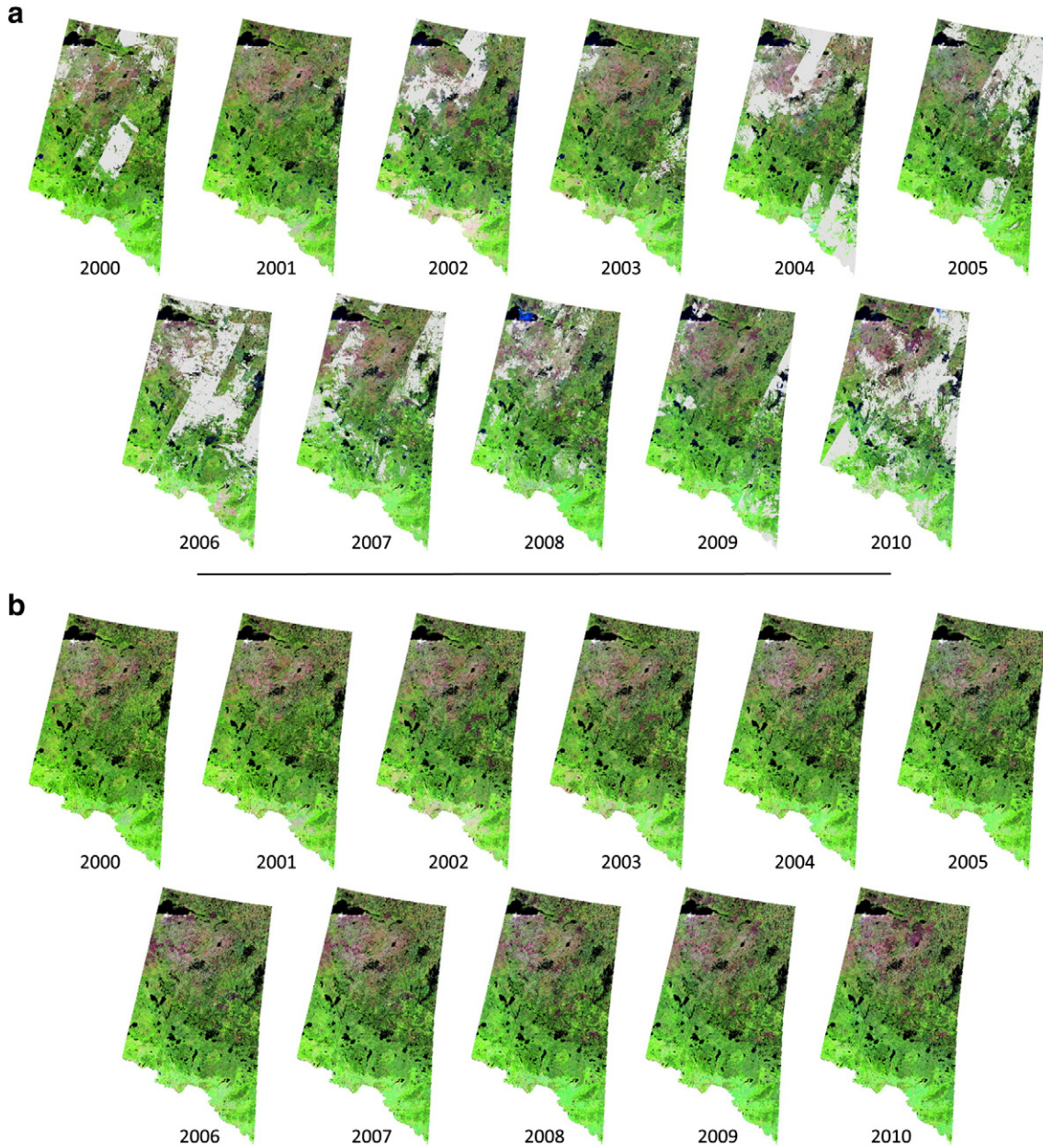


**Fig. 8.** (a) Annual image composites resulting from the BAP scoring showing the data gaps, and (b) annual image composites infilled with the proxy values for the whole study area.

of change annually), and where persistent, extensive cloud cover limits the availability of suitable imagery. In such circumstances, using spatial interpolation techniques to fill in data gaps may be considered as a complement to the lack of spectral information in the time series.

In addition to being an essential precursor to the assignment of appropriate proxy values, the breakpoint detection process results in the generation of a series of change metrics that have potential widespread utility for mapping, modeling, and characterizing land cover and land cover dynamics (Table 1). These metrics provide a comprehensive characterization of change events that can enable an improved understanding for monitoring purposes, particularly with regards to the severity, timing, and duration of various change processes in a region, as well as the pre- and post-change processes. For this study area in Saskatchewan, where the dominant change agent is wildfire, the outputs from the change metrics correspond to expectations for annual change in this boreal region (Delong & Tanner, 1996). Thus, while changes in the northern part of the study area region, which are typically large and persist

for only a single year, are most often caused by wildfires, changes located in the southern part of the study area, which are smaller and in some cases persist for more than a single year, are most often anthropogenic in origin (e.g., harvesting, post-insect infestation or fire salvage) (Masek et al., 2011; Schroeder, Wulder, Healey & Moisen, 2012).

The assignment of proxy values is complicated by the presence of change events in the pixel series. Currently only major events are captured when defining the segments from which the piecewise linear interpolation is performed, which may hinder the detection of smaller, more subtle disturbances and consequently create proxy values that do not accurately represent the true spectral values. Characterizing multiple disturbances within the pixel series may be particularly important when considering longer periods of time (e.g., 1990–2010). Additionally, extrapolation of values at the beginning and the end of the time series requires special attention; although, the extra years included in our process (1998–1999 and 2011–2012) are aimed at mitigating this issue.

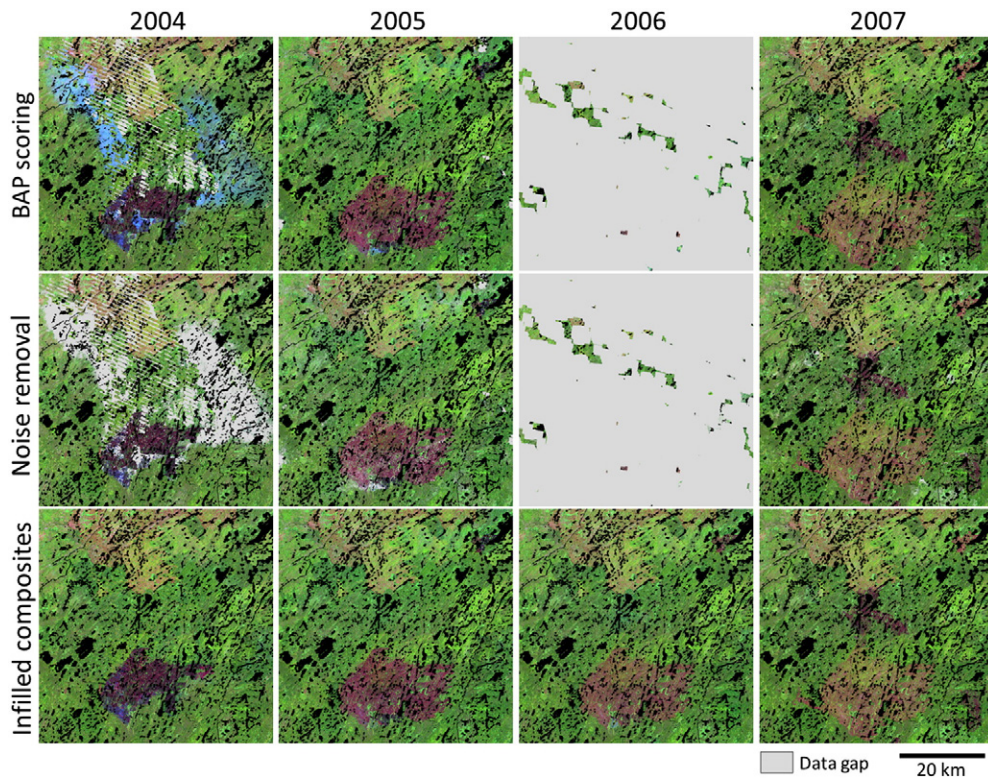


**Fig. 9.** Detail of the different phases of the image compositing process for the years 2004–2007. First and second row respectively show the data gaps resulting from the BAP scoring (included buffered clouds, shadows and haze, e.g., 2006) and noise removal processes (including residual clouds or smoke, e.g., 2004). Third row shows the final image composites infilled with the proxy values.

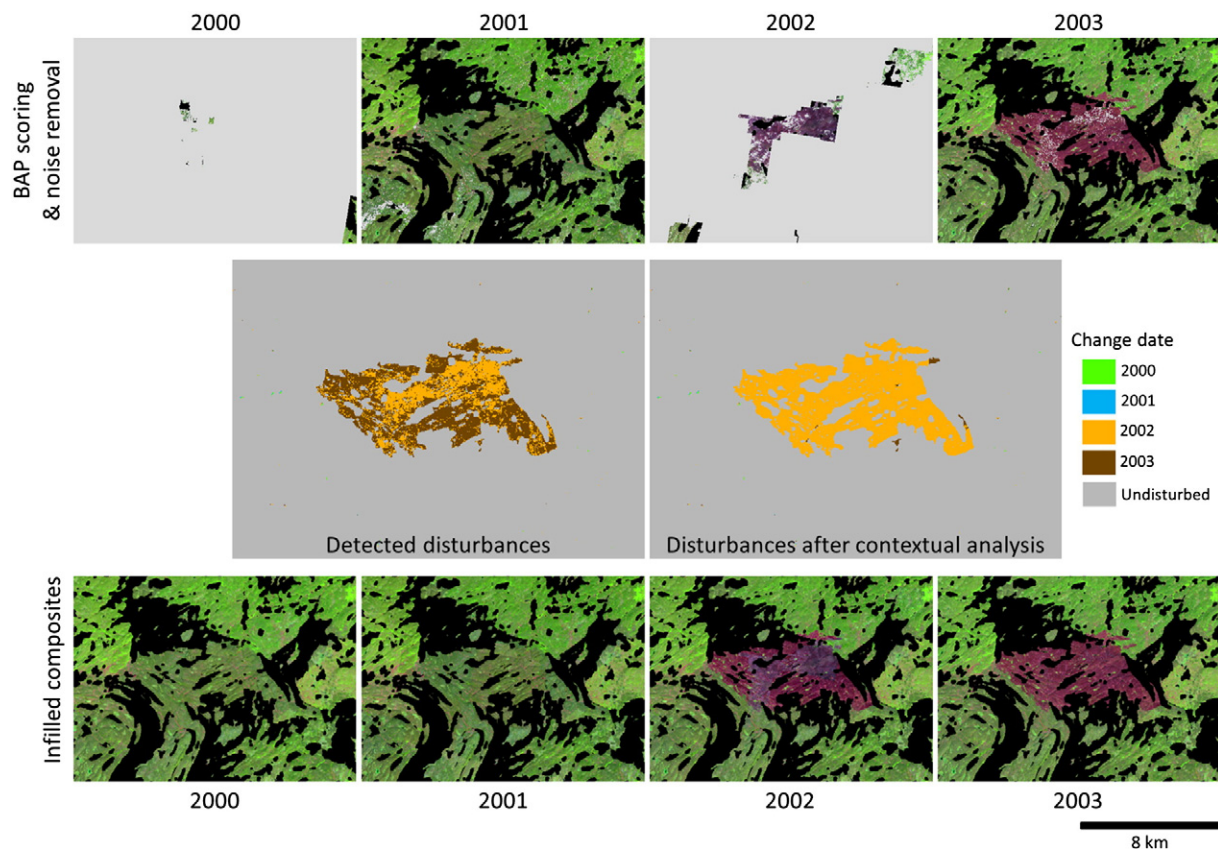


**Fig. 10.** Detail of the different phases of the image compositing process for the years 2000–2003. The first row shows the data gaps resulting from both the BAP scoring and noise removal processes. The second row shows the changes detected after the analysis of the pixel series (temporal domain), and after performing the contextual analysis (spatial domain). The third row shows the final image composites infilled with the proxy values.

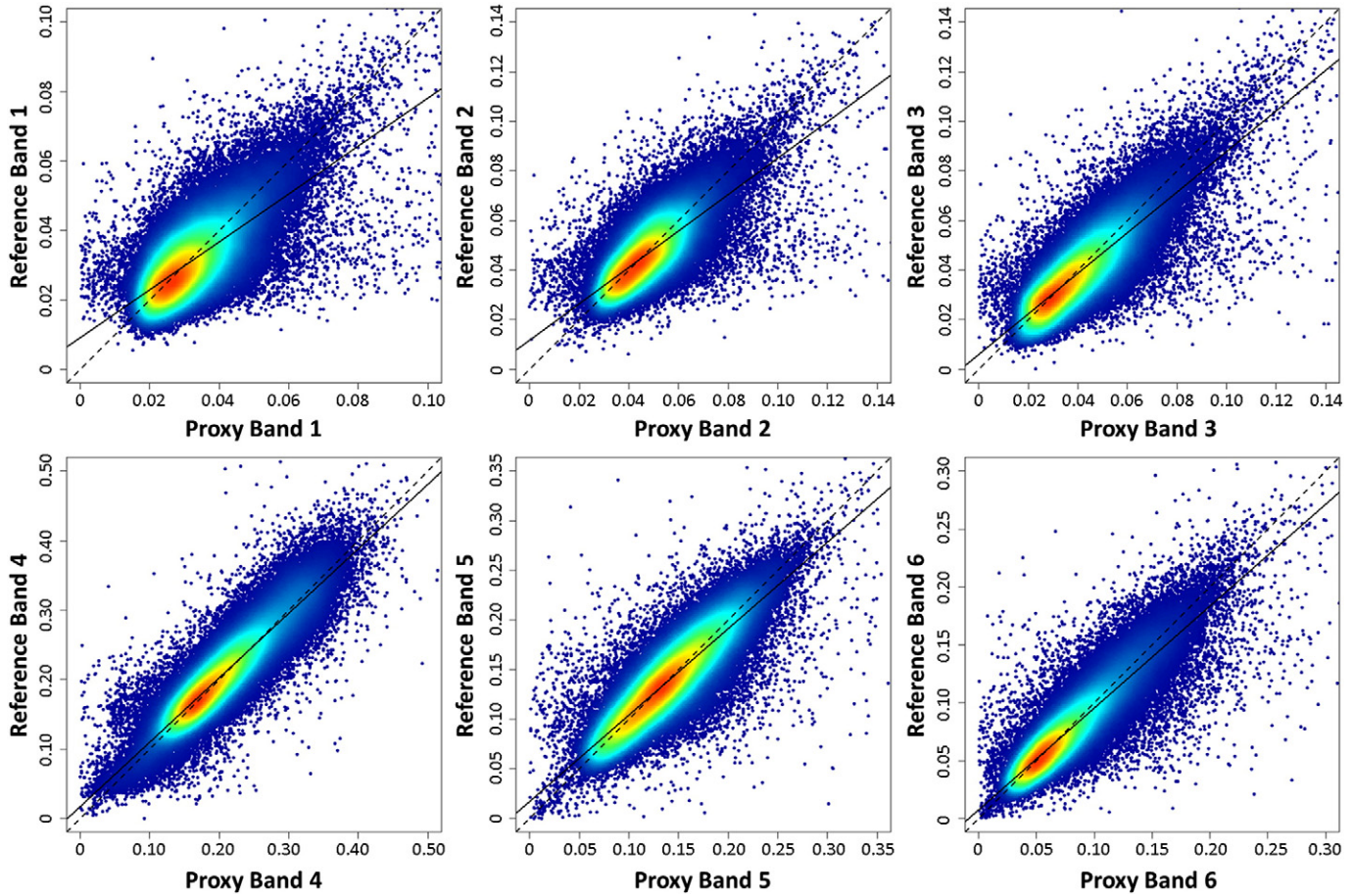


**Fig. 11.** Observed (reference) vs. predicted (proxy) values in surface reflectance units. Solid line represents the linear fitting and dotted line is the 1:1 line.

Lastly, data gaps constitute a major challenge for image compositing. In our example, the impact of data gaps was mitigated through the assignment of proxy values and the use of contextual information to aid in the correct labeling and characterization of disturbance events. A number of methods have been proposed in the literature to assign proxy values to data gaps including the use of alternate satellite imagery, such as SPOT (French: *Satellite Pour l'Observation de la Terre*, "Satellite for observation of Earth") or IRS (Indian Remote Sensing) (Gao, Masek, Schwaller, & Hall, 2006; Hilker et al., 2009; Rulloni, Bustos, & Flesia, 2012). When considering alternate imagery, it is necessary to recall that although some non-Landsat imagery fulfill certain baseline requirements that enable them to emulate Landsat image characteristics, it is unlikely that sufficient similarity exists to enable direct integration (Wulder, White, Masek, Dwyer, & Roy, 2011). Sentinel-2 to be launched in 2015 was developed to enable compatibility with Landsat (Drusch et al., 2012) and may offer an opportunity for direct incorporation of reflectance values for spatially and spectrally complementary channels. However, this will require further investigation to solve issues

such as matching different spectral bands' bandwidths or different spatial-resolution imagery integration. Satellites collecting data that are not subject to the same levels of radiometric calibration and spatial precision may not offer direct integration, but could be subject to some form of normalization to enable incorporation of imagery to a BAP process.

## 7. Conclusions

The remote sensing research community is currently discovering how best to exploit the massive amount of data available following the opening of the Landsat archive. These applications all take advantage of Landsat's temporal depth and global coverage to improve monitoring of terrestrial ecosystems. In this paper we presented a protocol that aims to bring together a number of change detection approaches from time series analyses (that are often undertaken on only a single or a limited number of scenes) as well as large area mapping methods (which can be spatially extensive but typically only relate epochal

**Table 2**

Assessment of proxy values relative to reference values for all pixels, no change pixels, and change pixels. Units for RMSE and bias are surface reflectance.

Band	All pixels					No change pixels					Change pixels				
	R	R <sup>2</sup>	RMSE	Bias	CV	R	R <sup>2</sup>	RMSE	Bias	CV	R	R <sup>2</sup>	RMSE	Bias	CV
1	0.72	0.51	0.0079	0.0008	25.42	0.73	0.54	0.0071	0.0008	23.76	0.63	0.39	0.0103	0.0008	29.33
2	0.76	0.57	0.0085	0.0008	18.47	0.79	0.62	0.0076	0.0008	16.65	0.68	0.46	0.0114	0.0007	23.36
3	0.84	0.71	0.0086	0.0012	22.49	0.86	0.74	0.0076	0.0012	20.63	0.76	0.57	0.0118	0.0012	26.36
4	0.91	0.83	0.0249	-0.0027	12.23	0.91	0.83	0.0238	-0.0027	11.22	0.87	0.76	0.0287	-0.0027	16.67
5	0.88	0.77	0.0202	0.0007	14.78	0.90	0.81	0.0171	0.0006	12.85	0.78	0.61	0.0291	0.0013	19.25
7	0.91	0.82	0.0151	0.0011	20.37	0.92	0.85	0.0119	0.0010	17.43	0.84	0.71	0.0236	0.0018	24.46

**Table 3**

Assessment of proxy values relative to reference values in the context of an increasing number of data gaps, as well as an increasing number of consecutive data gaps. Results are presented for band 4 only (although trends for other bands are similar). Units for RMSE and bias are surface reflectance.

Number of years	With data gaps						With consecutive data gaps					
	R	R <sup>2</sup>	RMSE	Bias	CV	Number of samples	R	R <sup>2</sup>	RMSE	Bias	CV	Number of samples
0	0.92	0.85	0.0269	-0.0022	12.36	6687	0.92	0.85	0.0269	-0.0022	12.36	6687
1	0.92	0.85	0.0255	-0.0024	12.07	14472	0.92	0.85	0.0245	-0.0028	11.92	66275
2	0.92	0.85	0.0245	-0.0028	11.92	20523	0.90	0.81	0.0248	-0.0029	12.44	31586
3	0.91	0.83	0.0244	-0.0029	11.94	23897	0.89	0.79	0.0244	-0.0025	12.50	9087
4	0.90	0.81	0.0244	-0.0029	12.14	21561	0.83	0.69	0.0293	-0.0023	15.08	2138
5	0.90	0.81	0.0245	-0.0029	12.37	15361	0.74	0.55	0.0365	-0.0007	19.24	399
6	0.88	0.77	0.0251	-0.0027	12.88	8599	0.79	0.62	0.0325	-0.0014	17.22	143
7	0.87	0.76	0.0253	-0.0027	13.26	3599	0.81	0.66	0.0399	-0.0064	19.73	33
8	0.85	0.72	0.0269	-0.0028	14.19	1159	0.79	0.62	0.0250	0.0119	15.81	24
9	0.79	0.62	0.0340	-0.0013	18.33	300	0.50	0.25	0.0511	0.0184	31.16	9
10	0.83	0.69	0.0297	0.0040	17.22	81	-0.72	0.52	0.0706	0.0366	44.31	4
11	0.87	0.76	0.0284	-0.0040	15.36	30	0.80	0.64	0.0261	-0.0006	11.13	3

changes, rather than accounting for annual changes). The BAP compositing process generates image composites through an approach that is pixel-based rather than scene-based. A portion of the pixels in these BAP composites are either missing observations or have noisy or anomalous values. The protocol presented herein – using Landsat TM and ETM + data – enables the production of spatially contiguous, cloud- and haze-free, spectrally-consistent, temporal series of proxy surface reflectance composites. As an important precursor to proxy value assignment, the protocol analyzes the spectral reflectance values of the pixels through time and generates a set of change metrics that characterize the year, persistence, rates of change, severity, recovery, rates of recovery, as well as the pre- and post-change event scenarios. These proxy composites, together with the change metrics, provide valuable independent information for systematically mapping, monitoring, and reporting physical characteristics of land cover, land-cover changes and related dynamics over large areas for extended time periods at regional or national levels. These outcomes can be used as model inputs, such as in support of carbon budget modeling, providing extensive information to resource managers and decision-makers to assist the development and application of policies for enhanced land management. Future work will focus on the application of the protocol to different areas and further improvements to the change metrics (and thereby the proxy values) by allowing for multiple change events within the pixel series to be identified and characterized. In addition, we are actively exploring the use of these proxy value composites and change metrics to characterize land cover, land cover change, and vertical forest structure.

## Acknowledgments

This research was undertaken as part of the “National Terrestrial Ecosystem Monitoring System (NTEMS): Timely and detailed national cross-sector monitoring for Canada” project jointly funded by the Canadian Space Agency (CSA) Government Related Initiatives Program (GRIP) and the Canadian Forest Service (CFS) of Natural Resources Canada. We thank the anonymous reviewers and the editor for their valuable comments and suggestions to improve the manuscript.

## References

- Brooks, E. B., Thomas, V. A., Wynne, R. H., & Coulston, J. W. (2012). Fitting the multitemporal curve: A Fourier series approach to the missing data problem in remote sensing analysis. *IEEE Transactions on Geoscience and Remote Sensing*, 50(9), 3340–3353. <http://dx.doi.org/10.1109/TGRS.2012.2183137>.
- Chen, J. (2004). A simple method for reconstructing a high-quality NDVI time-series data set based on the Savitzky–Golay filter. *Remote Sensing of Environment*, 91(3–4), 332–344. <http://dx.doi.org/10.1016/j.rse.2004.03.014>.
- Cohen, W. B., & Goward, S. N. (2004). Landsat's role in ecological applications of remote sensing. *BioScience*, 54(6), 535. [http://dx.doi.org/10.1641/0006-3568\(2004\)054\[0535:LRIOAO\]2.0.CO;2](http://dx.doi.org/10.1641/0006-3568(2004)054[0535:LRIOAO]2.0.CO;2).
- Cohen, W. B., Spies, T. a, Alig, R. J., Oetter, D. R., Maiersperger, T. K., & Fiorella, M. (2002). Characterizing 23 years (1972–95) of stand replacement disturbance in Western Oregon forests with Landsat imagery. *Ecosystems*, 5(2), 122–137. <http://dx.doi.org/10.1007/s10021-001-0060-X>.
- Delong, S. C., & Tanner, D. (1996). Managing the pattern of forest harvest: Lessons from wildlife. *Biodiversity and Conservation*, 5.
- Drusch, M., Del Bello, U., Carlier, S., Colin, O., Fernandez, V., Gascon, F., et al. (2012). Sentinel-2: ESA's optical high-resolution mission for GMES operational services. *Remote Sensing of Environment*, 120, 25–36. <http://dx.doi.org/10.1016/j.rse.2011.11.026>.
- Flood, N. (2013). Seasonal composite Landsat TM/ETM + images using the Medoid (a multi-dimensional median). *Remote Sensing*, 5(12), 6481–6500. <http://dx.doi.org/10.3390/rs5126481>.
- Gao, F., Masek, J. G., Schwaller, M., & Hall, F. (2006). On the blending of the Landsat and MODIS surface reflectance: Predicting daily Landsat surface reflectance. *IEEE Transactions on Geoscience and Remote Sensing*, 44(8), 2207–2218. <http://dx.doi.org/10.1109/TGRS.2006.872081>.
- Geerken, R., Zaitchik, B., & Evans, J. P. (2005). Classifying rangeland vegetation type and coverage from NDVI time series using Fourier filtered cycle similarity. *International Journal of Remote Sensing*, 26(24), 5535–5554. <http://dx.doi.org/10.1080/01431160500300297>.
- Griffiths, P., Linden, S., Van Der Kuemmerle, T., & Hostert, P. (2013). A pixel-based Landsat compositing algorithm for large area land cover mapping. *IEEE Journal of Selected Topics in Applied Earth Observations and Remote Sensing*, 6(5), 2088–2101.
- Hansen, M. C., Egorov, A., Roy, D. P., Potapov, P., Ju, J., Turubanova, S., et al. (2011). Continuous fields of land cover for the conterminous United States using Landsat data: First results from the Web-Enabled Landsat Data (WELD) project. *Remote Sensing Letters*, 2(4), 279–288. <http://dx.doi.org/10.1080/01431161.2010.519002>.
- Hansen, M. C., & Loveland, T. R. (2012). A review of large area monitoring of land cover change using Landsat data. *Remote Sensing of Environment*, 122, 66–74. <http://dx.doi.org/10.1016/j.rse.2011.08.024>.
- Hilker, T., Wulder, M. A., Coops, N. C., Seitz, N., White, J. C., Gao, F., et al. (2009). Generation of dense time series synthetic Landsat data through data blending with MODIS using a spatial and temporal adaptive reflectance fusion model. *Remote Sensing of Environment*, 113(9), 1988–1999. <http://dx.doi.org/10.1016/j.rse.2009.05.011>.
- Huang, C., Goward, S. N., Masek, J. G., Thomas, N., Zhu, Z., & Vogelmann, J. E. (2010). An automated approach for reconstructing recent forest disturbance history using dense Landsat time series stacks. *Remote Sensing of Environment*, 114(1), 183–198. <http://dx.doi.org/10.1016/j.rse.2009.08.017>.
- Jönsson, P., & Eklundh, L. (2004). TIMESAT—A program for analyzing time-series of satellite sensor data. 1. *Computers & Geosciences*, 30(8), 833–845. <http://dx.doi.org/10.1016/j.cageo.2004.05.006>.
- Ju, J., Roy, D. P., Shuai, Y., & Schaaf, C. (2010). Development of an approach for generation of temporally complete daily nadir MODIS reflectance time series. *Remote Sensing of Environment*, 114(1), 1–20. <http://dx.doi.org/10.1016/j.rse.2009.05.022>.
- Kennedy, R. E., Cohen, W. B., & Schroeder, T. A. (2007). Trajectory-based change detection for automated characterization of forest disturbance dynamics. *Remote Sensing of Environment*, 110, 370–386. <http://dx.doi.org/10.1016/j.rse.2007.03.010>.
- Kennedy, R. E., Yang, Z., & Cohen, W. B. (2010). Detecting trends in forest disturbance and recovery using yearly Landsat time series: 1. LandTrendr – Temporal segmentation algorithms. *Remote Sensing of Environment*, 114, 2897–2910. <http://dx.doi.org/10.1016/j.rse.2010.07.008>.
- Keogh, E., Chu, S., Hart, D., & Pazzani, M. (2001). *An online algorithm for segmenting time series*. *Data mining, 2001. ICDM*, 289–296. <http://dx.doi.org/10.1109/ICDM.2001.989531>.
- Key, C. H., & Benson, N. C. (2006). *Landscape assessment (LA): Sampling and analysis methods*. USDA Forest Service Gen. Tech. Rep. RMRS-GTR-164-CD.
- Liang, S., Fang, H., & Morissette, J. T. (2002). Atmospheric correction of Landsat ETM + land surface imagery. II. Validation and applications. *IEEE Transactions on Geoscience and Remote Sensing*, 40(12), 2736–2746. <http://dx.doi.org/10.1109/TGRS.2002.807579>.
- Lou, Q., & Obradovic, Z. (2011). Modeling multivariate spatio-temporal remote sensing data with large gaps. *IJCAI Proceedings-International Joint Conference on Artificial Intelligence* (pp. 1711–1716) (Barcelona, Spain. Retrieved from <http://www.aaai.org/ocs/index.php/IJCAI/IJCAI11/paper/viewPDFInterstitial/3041/3773>.

- Loveland, T. R., & Dwyer, J. L. (2012). Landsat: Building a strong future. *Remote Sensing of Environment*, 122(October 2000), 22–29. <http://dx.doi.org/10.1016/j.rse.2011.09.022>.
- Lunetta, R. S., Johnson, D. M., Lyon, J. G., & Crotwell, J. (2004). Impacts of imagery temporal frequency on land-cover change detection monitoring. *Remote Sensing of Environment*, 89(4), 444–454.
- Masek, J. G., Cohen, W. B., Leckie, D., Wulder, M. A., Vargas, R., de Jong, B., et al. (2011). Recent rates of forest harvest and conversion in North America. *Journal of Geophysical Research*, 116(G4), 1–22. <http://dx.doi.org/10.1029/2010G001471>.
- Masek, J. G., Vermote, E. F., Saleous, N. E., Wolfe, R., Hall, F. G., Huemmrich, K. F., et al. (2006). A Landsat surface reflectance dataset for North America, 1990–2000. *IEEE Geoscience and Remote Sensing Letters*, 3(1), 68–72.
- McKenney, D., Pedlar, J., Papadopol, P., & Hutchinson, M. (2006). The development of 1901–2000 historical monthly climate models for Canada and the United States. *Agricultural and Forest*, 138(1–4), 69–81. <http://dx.doi.org/10.1016/j.agrformet.2006.03.012>.
- Meissner, R. E., Bittner, M., & Dech, S. W. (1999). Computer animation of remote sensing-based time series data sets. *IEEE Transactions on Geoscience and Remote Sensing*, 37(2), 1100–1106. <http://dx.doi.org/10.1109/36.752228>.
- Potapov, P., Turubanova, S., & Hansen, M. C. (2011). Regional-scale boreal forest cover and change mapping using Landsat data composites for European Russia. *Remote Sensing of Environment*, 115(2), 548–561. <http://dx.doi.org/10.1016/j.rse.2010.10.001>.
- Pflugmacher, D., Cohen, W. B., Kennedy, R. E., & Yang, Z. (2014). Using Landsat-derived disturbance and recovery history and lidar to map forest biomass dynamics. *Remote Sensing of Environment*, 151, 124–137.
- Roerink, G. J., Mementi, M., & Verhoeef, W. (2001). International Journal of Reconstructing cloudfree NDVI composites using Fourier analysis of time series. *International Journal of Remote Sensing*, 21(9), 1911–1917.
- Rowe, J. S. (1996). Land classification and ecosystem classification. *Environmental Monitoring and Assessment*, 39(1–3), 11–20. <http://dx.doi.org/10.1007/BF00396131>.
- Roy, D. P., Ju, J., Kline, K., Scaramuzza, P. L., Kovalsky, V., Hansen, M., et al. (2010). Web-enabled Landsat Data (WELD): Landsat ETM + composited mosaics of the conterminous United States. *Remote Sensing of Environment*, 114(1), 35–49. <http://dx.doi.org/10.1016/j.rse.2009.08.011>.
- Rulloni, V., Bustos, O., & Flesia, A. G. (2012). Large gap imputation in remote sensed imagery of the environment. *Computational Statistics and Data Analysis*, 56(8), 2388–2403. <http://dx.doi.org/10.1016/j.csda.2012.02.022>.
- Schmidt, G. L., Jenkerson, C. B., Masek, J., Vermote, E., & Gao, F. (2013). *Landsat ecosystem disturbance adaptive processing system (LEDAPS) algorithm description*. 17 (Retrieved from <http://pubs.usgs.gov/of/2013/1057/>).
- Schroeder, T. A., Wulder, M. A., Healey, S. P., & Moisen, G. G. (2012). Detecting post-fire salvage logging from Landsat change maps and national fire survey data. *Remote Sensing of Environment*, 122, 166–174. <http://dx.doi.org/10.1016/j.rse.2011.10.031>.
- Tomé, A. R., & Miranda, P. M. A. (2004). Piecewise linear fitting and trend changing points of climate parameters. *Geophysical Research Letters*, 31(2), L02207. <http://dx.doi.org/10.1029/2003GL019100>.
- Townshend, J., Latham, J., Justice, C. O., Janetos, A., Conant, R., Arino, O., et al. (2011). *Land Remote Sensing and Global Environmental Change*, 11, 835–856. <http://dx.doi.org/10.1007/978-1-4419-6749-7>.
- Verbesselt, J., Hyndman, R., Zeileis, A., Culvenor, D. S., & Newnham, G. J. (2010). Detecting trend and seasonal changes in satellite image time series. *Remote Sensing of Environment*, 114(1), 106–115. <http://dx.doi.org/10.1016/j.rse.2010.08.003>.
- Vicente-Serrano, S., Perez-Cabello, F., & Lasanta, T. (2008). Assessment of radiometric correction techniques in analyzing vegetation variability and change using time series of Landsat images. *Remote Sensing of Environment*, 112(10), 3916–3934. <http://dx.doi.org/10.1016/j.rse.2008.06.011>.
- White, J., & Wulder, M. (2013). The Landsat observation record of Canada: 1972–2012. *Canadian Journal of Remote Sensing*, 39(6), 455–467. <http://dx.doi.org/10.1080/01431161.2013.779041>.
- White, J. C., Wulder, M. A., Hobart, G. W., Luther, J. E., Hermosilla, T., Griffiths, P., et al. (2014). Pixel-based image compositing for large-area dense time series applications and science. *Canadian Journal of Remote Sensing*, 40(3), 192–212. <http://dx.doi.org/10.1080/07038992.2014.945827>.
- Wulder, M. A., Bater, C. W., Coops, N. C., Hilker, T., & White, J. C. (2008). The role of LiDAR in sustainable forest management. *The Forestry Chronicle*, 84(6), 807–826.
- Wulder, M. A., White, J. C., Goward, S. N., Masek, J. G., Irons, J. R., Herold, M., et al. (2008). Landsat continuity: Issues and opportunities for land cover monitoring. *Remote Sensing of Environment*, 112(3), 955–969. <http://dx.doi.org/10.1016/j.rse.2007.07.004>.
- Wulder, M. A., White, J. C., Masek, J. G., Dwyer, J., & Roy, D. P. (2011). Continuity of Landsat observations: Short term considerations. *Remote Sensing of Environment*, 115(2), 747–751. <http://dx.doi.org/10.1016/j.rse.2010.11.002>.
- Zhou, L., Tucker, C., Kaufmann, R. K., Slayback, D., Shabanov, N. V., & Myneni, R. B. (2001). Variations in northern vegetation activity inferred from satellite data of vegetation index during 1981 to 1999. *Journal of Geophysical Research*, 106(D17), 20069–20083. <http://dx.doi.org/10.1029/2000JD000115/full>.
- Zhu, Z., & Woodcock, C. E. (2012). Object-based cloud and cloud shadow detection in Landsat imagery. *Remote Sensing of Environment*, 118, 83–94. <http://dx.doi.org/10.1016/j.rse.2011.10.028>.
- Zhu, Z., & Woodcock, C. E. (2014). Automated cloud, cloud shadow, and snow detection in multitemporal Landsat data: An algorithm designed specifically for monitoring land cover change. *Remote Sensing of Environment*, 152, 217–234. <http://dx.doi.org/10.1016/j.rse.2014.06.012>.
- Zhu, Z., Woodcock, C. E., & Olofsson, P. (2012). Continuous monitoring of forest disturbance using all available Landsat imagery. *Remote Sensing of Environment*, 122, 75–91. <http://dx.doi.org/10.1016/j.rse.2011.10.030>.